Materials Research. 2017; 20(1): 36-45
DOI: http://dx.doi.org/10.1590/1980-5373-MR-2015-0731

$CdMoO_4$ Micro-ellipsoids: Controllable Synthesis, Growth Mechanism, and Photocatalytic Activity

Ke Dai[a], Hui Liu[b], Tianyu Gao[a], Qi Wang[c], Hao Chen[b]*

[a] *College of Resources and Environment, Huazhong Agricultural University, Hubei, Wuhan, China*
[b] *College of Science, Huazhong Agricultural University, Hubei, Wuhan, China*
[c] *School of Environment Sciences and Engineering, Zhejiang Gongshang University, Zhejiang, Hangzhou, China*

Received: November 30, 2015; Revised: February 20, 2016; Accepted: November 3, 2016

$CdMoO_4$ micro-ellipsoids were synthesized by a simple hydrothermal route with the assistance of nonionic surfactant Triton X-100 and characterized by X-ray diffraction, scanning electron microscopy and UV-Vis diffuse reflectance spectroscopy. The effects of hydrothermal pH, temperature, and time on the morphology and photocatalytic activity of $CdMoO_4$ were investigated. With an initial hydrothermal pH of 5.00, $CdMoO_4$ micro-ellipsoids were obtained at 180 °C for 24 h and found to possess the highest photocatalytic activity—89% Rhodamine B can be degraded for 30 minutes presented in the 0.4 g/L $CdMoO_4$ suspension. The formation mechanism of the $CdMoO_4$ micro-ellipsoids was initiated by the formation of small nanoparticles and bulk structures afterwards, which was followed by the growth of micro-ellipsoids. Experiment results showed that the evolution of the micro-ellipsoids was an Ostwald ripening process.

Keywords: *photocatalysis, $CdMoO_4$, controllable synthesis, Ostwald ripening*

1. Introduction

The controllable synthesis of microscale and nanoscale materials with special morphology, architecture and properties have rapidly developed into a promising field in material chemistry[1-7]. Controlling synthesis conditions can generate different material structures, and changes in these structure directly affect their properties. Therefore, preparing materials with special morphologies and illustrating the growth mechanisms are particularly interesting, and *vice versa*, we can control synthesis of the required materials once growth mechanisms are clear.

Metal molybdates ($MMoO_4$, M=Zn^{2+}, Ni^{2+}, Pb^{2+}, Cd^{2+}, Sr^{2+}, et al.), as a kind of novel materials, are attracting increasing attention because of their excellent optical and electrical properties, high surface energy, numerous active sites, and high selectivity[8-11], As an important metal molybdate, $CdMoO_4$ is receiving considerable attention because of its electronic excitation with vacuum ultraviolet synchrotron radiation[12], pressure-induced phase transformations[13], and photocatalytic activities[14,15]. Therefore, synthetic methods and conditions of cadmium molybdate with high photocatalytic activity are significant to explore. Over the last few years, a few efforts have been exerted to the exploration some approaches to the fabrication of $CdMoO_4$ micro/nanostructures with special characters[16,17]. For example, Khademolhoseini et al.[18] synthesized $CdMoO_4$ with an ultrasonic method and found that the size and morphology of the products were greatly influenced by the dosage of ultrasonic power. Wang et al.[19] prepared 3D $CdMoO_4$ hierarchical structures from nanoplates with enhanced photocatalytic efficiency in the degradation of Rhodamine B under ultraviolet (UV) light irradiation. Li et al.[20] introduced Cl^- to the hydrothermal process and successfully obtained self-assembled $CdMoO_4$ microspheres that were used to degrade methylene blue. Li and Gong[21] prepared octahedral $CdMoO_4$ through different microemulsion systems. Wang et al.[22] designed a kind of $CdMoO_4$ microspheres with a core-shell structure and investigated the photocatalytic activity and fluorescence properties of the microspheres. Liu et al.[23] synthesized $CdMoO_4$ nanorods with the diameter of 30-50 nm at a relatively low temperature.

Based on the above mentioned studies, considerable attention has been paid to the controllable synthesis of molybdate cadmium with special morphology. However, studies on the relationship among the synthesis conditions (pH, temperature, and reaction time), morphologies, and photocatalytic activity of molybdate cadmium are few. In this work, we demonstrated a simple and efficient hydrothermal procedure for fabricating micro-ellipsoids $CdMoO_4$ by simply reacting ammonium molybdate with cadmium nitrate aqueous solution in the presence of Triton X-100. Micro-ellipsoids $CdMoO_4$ were selectively prepared by adjusting the hydrothermal temperature, reaction time, and pH. The photocatalytic activities of $CdMoO_4$ with various morphologies synthesized under different conditions were comparatively investigated by Rhodamine B (RhB) degradation. The growth process of micro-ellipsoids $CdMoO_4$ was also investigated in detail.

* e-mail: hchenhao@mail.hzau.edu.cn

2. Experimental

2.1. Materials

Cadmium acetate ($Cd(NO_3)_2$•$4H_2O$, AR.), ammonium molybdate ($(NH_4)_6Mo_7O_{24}$•$4H_2O$, AR.) and Triton X-100 (OP, CP.) were all purchased from Sinopharm Chemical Reagent Co. Ltd. without further purification. The water used in this experiment was deionized water.

2.2. Preparation of $CdMoO_4$

In a typical synthetic procedure, 14 mL 0.14 mol/L $Cd(NO_3)_2$•$4H_2O$ aqueous solution was completely dropwise dispersed in the mixed solution of 14 mL 0.02 mol/L $(NH_4)_6Mo_7O_{24}$•$4H_2O$ and Triton X-100 under vigorous stirring. Subsequently, the mixed solution was adjusted to various pH value (1.73, 3.00, 5.00, 7.00, 9.00, and 11.00) with an ammonia solution or nitric acid solution. Then, the mixture was transferred into a Teflon-lined stainless steel autoclave and heated in the oven according to the setting time (1, 4, 8, 12, 16, 20, 24, 36, and 48 h) and temperature (25, 50, 70, 80, 100, 140, and 180 °C). Unless otherwise stated, the reaction conditions of pH, temperature, and time are set at pH=5.00, 180 °C for 24 h. Finally, the resultant solid was separated by centrifugation and washed with deionized water and ethanol three times and then dried at 80 °C for 8 h in the air.

2.3. Characterizations

X-ray diffraction (XRD) patterns were collected on a Bruker D8 advance X-ray diffractometer with Cu Kα radiation (λ=0.15406 nm). The UV-vis diffuse reflectance spectroscopy of power solids were carried out by UV-Vis spectrophotometer (UV-3100, Japan), made by Japan. The morphologies were studied with a JSM-6390LV scanning electron microscope (SEM).

2.4. Photocatalytic experiments

Photocatalytic activities were evaluated by the degradation of RhB under UV light irradiation of an 18 W mercury lamp (average light intensity of 14.5 $\mu W/cm^2$). In each experiment, 20 mg of photocatalysts was added into 50 mL of RhB solution (1×10^{-5} mol/L). Before irradiation, the suspensions were magnetically stirred in the dark for 30 min to achieve the adsorption equilibrium. Then the suspensions were exposed to UV light irradiation. At given irradiation time intervals, 3 mL of the suspension was collected and centrifuged to remove the photocatalyst. The centrifuged solution was analyzed by a Nicolet 300 evolution UV-vis spectrophotometer, monitoring the characteristic absorption peak of RhB at 553 nm.

3. Results and discussion

3.1. XRD analyses of $CdMoO_4$ microcrystals

Figure 1 shows the XRD patterns of $CdMoO_4$ microcrystals. Figure 1b-1d show the XRD patterns of various $CdMoO_4$ products prepared at different hydrothermal temperatures, times, and pH values, respectively. All diffraction peaks of the XRD patterns (Figure 1b-1d) can be ascribed to tetragonal-phase $CdMoO_4$ (JCPDS no: 07-0209). The peaks at 29.2°, 31.9°, 34.8°, 47.9° and 59.0° show an excellent match with the (112), (004), (200), (204), (312) crystal planes of tetragonal-phase $CdMoO_4$, indicating that all samples were tetragonal-phase $CdMoO_4$ (Figure 1a). Figure 1b shows that the diffraction peak intensity strengthens and sharpens with increased temperature, indicating the crystallinity increases with increased temperature and time[24,25]. Moreover, the diffraction peak intensity ratios (I_{004}/I_{200}) of the (004) and (200) crystal planes are calculated to be 0.7, 1.9, and 3.6 for the sample prepared at 70, 140, and 180 °C, respectively. Therefore, the microcrystals undergo special anisotropic growth along the c-axis with increased hydrothermal temperature from 70 °C to 180 °C[26,27]. Figure 1c shows that the crystallinity increases with increased time, indicating special anisotropic growth along the c-axis with prolonged hydrothermal time from 8 h to 24 h. Figure 1d shows that the crystals' orientation does not significantly change when the pH is changed, but pH has an important effect on morphology of $CdMoO_4$ crystals[16], as also can be investigated in Section 3.2. Thus, crystal-growth orientation, morphology and crystallinity can be controlled by hydrothermal temperature, reaction time, and pH.

3.2. $CdMoO_4$ morphologies analyses

The SEM images of $CdMoO_4$ products obtained at different hydrothermal temperatures for 24 h are shown in Figure 2. The hydrothermal temperature significantly affects the morphology of products. $CdMoO_4$ microparticles derived at 50 °C with an irregular shape can be observed in Figure 2a. The panoramic view in Figure 2b clearly illustrates that $CdMoO_4$ hydrothermally derived at 70 °C mostly consists of relatively uniform microspheres with diameters of 2-8 μm, coexisting with many irregular nanoparticles. One individual microsphere, as can be clearly observed from the inset in Figure 2b, has a well-defined spherical shape with a diameter of ca. 7 μm. Figure 2c shows that the microspheres derived at 80 °C possibly consist of aggregations containing nanoparticles and nanosheets. Similar rod-like morphologies of the products derived at 100 and 140 °C can be clearly observed in Figure 2d and 2e, and this finding can be attributed to the crushing of microspheres at the higher temperature. In the Figure 2f, products with irregular shapes are revealed because of agglomeration at 180 °C.

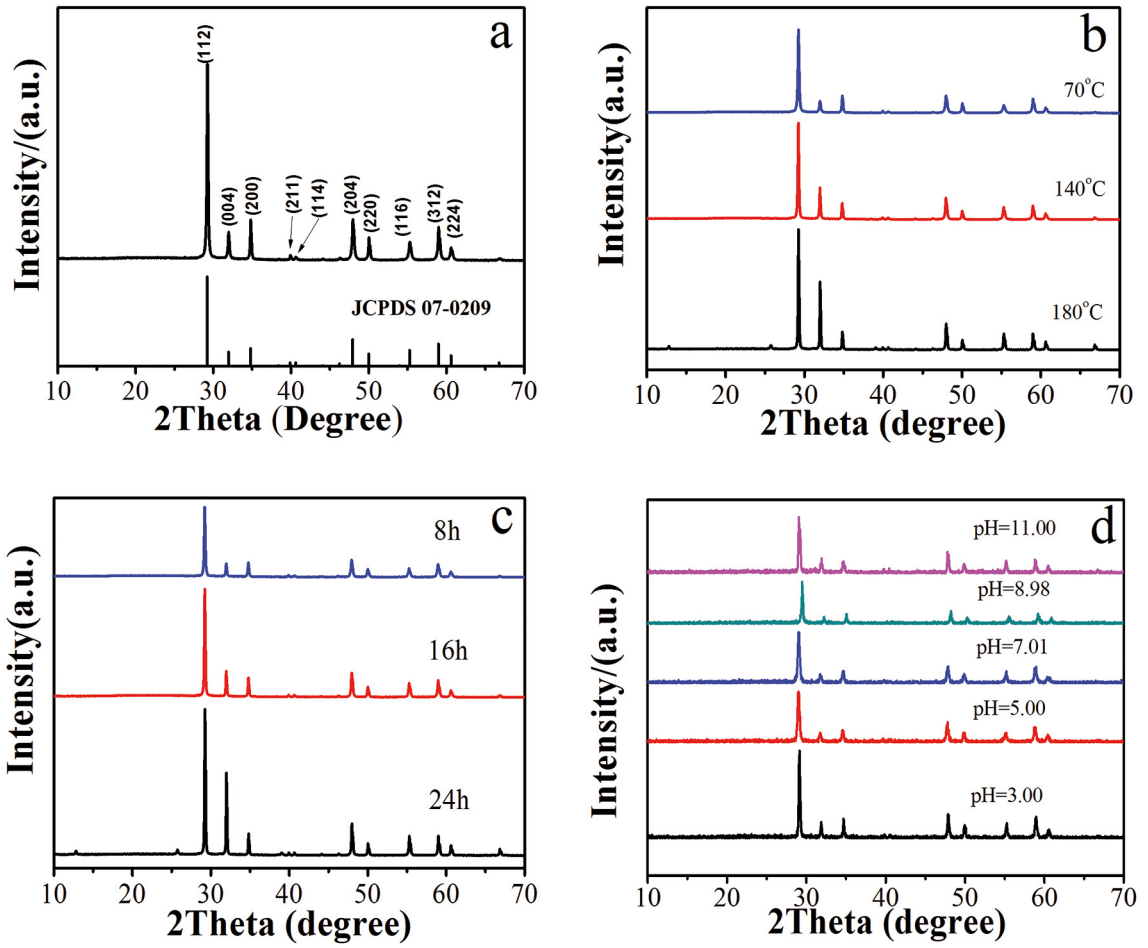

Figure 1: XRD pattern of the as-prepared $CdMoO_4$ products. (a) JCPDS 07-0209, (b) temperature series at pH=5 for 24 h, (c) time series at pH=5 and 180 °C, and (d) pH series at 70 °C for 24 h.

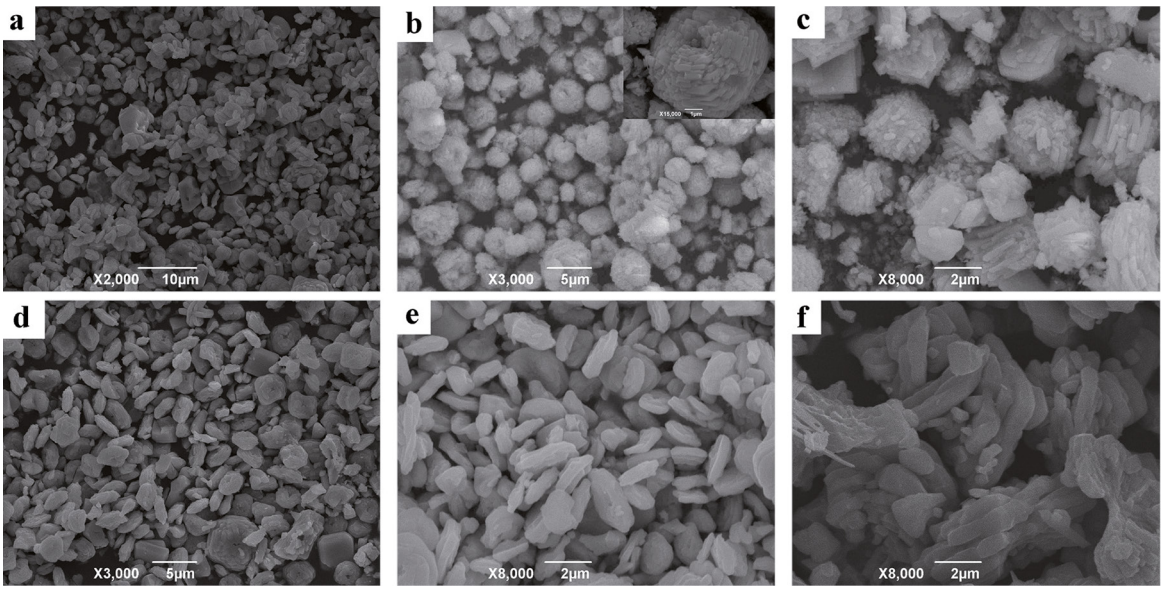

Figure 2: SEM images of $CdMoO_4$ products obtained at pH=5 for 24 h under different hydrothermal temperatures. (a) 50 °C, (b) 70 °C, (c) 80 °C, (d) 100 °C, (e) 140 °C, and (f) 180 °C.

Many researchers reported that $CdMoO_4$ materials have been synthesized at a low temperature[16,21,22]. To obtain $CdMoO_4$ materials with high crystallinity degree at a relatively benign synthetic condition, we synthetized $CdMoO_4$ particles at 180 °C. Moreover, the growth process of $CdMoO_4$ at 180 °C was investigated in this work, SEM images of $CdMoO_4$ products obtained at different growth stages at 180 °C are shown in Figure 3. After 1 h of hydrothermal reaction, products with square pieces are observed (Figure 3a), and the map inset is a well-defined square piece with a side length of ~3.6 μm and a thickness of ~500 nm. Apparently, the most exposed surface of the square piece is the crystal facet. As the reaction proceeded, a round pie shape with an average thickness of ~1.5 μm and diameters ranging within 2-3 μm is observed (Figure 3b). When the reaction time is prolonged to 8 h, the morphology type is still round pie shape but with an average thickness of ~1.2 μm and an average diameter of 3.3 μm (Figure 3c). When the reaction time is 1-8 h, morphological evolution of the crystal indicates that $CdMoO_4$ grows layer-by-layer from the sheet structure to round pie shape along the c-axis. Therefore, $CdMoO_4$ crystals grow along the c-axis perpendicular to the crystal facet, as can be observed from the SEM images (Figure 3a-3c). Finally, when the reaction time is further extended to 16, 24, even 48 h, regular crystal structures began to collapse or even seriously agglomerate, as shown in Figure 3d-3f.

$CdMoO_4$ microcrystals obtained at different pH values after hydrothermal treatment at 180 °C for 24 h were carefully examined by SEM. At pH 1.73, irregular nanoscale shapes are observed (Figure 4a). At pH 3.00, many nanospheres exist on the surface of block structures (Figure 4b). At pH 5.00, the as-prepared $CdMoO_4$ crystallites are well-defined micro-ellipsoids 3-5 μm in size (Figure 4c). At pH 7.00, the morphology is ellipsoid but many nanoparticles exist on their surface (Figure 4d). At pH 9.00, irregular lumps can be observed (Figure 4e). "Floccule"-like $CdMoO_4$ crystallites appear at pH 11.00 (Figure 4f).

3.3. Optical properties, photocatalytic activities and photostability

Optical absorption of the $CdMoO_4$ microparticles was measured by using an UV-vis spectrometer. Figure 5 presents a typical UV-vis diffuse reflectance absorption spectra (DRS) of $CdMoO_4$ products. The optical absorption of the $CdMoO_4$ microcrystals was nearly the same except the sample obtained at pH=11.00 (Figure 5c). All samples show a great increase in absorbance with wavelengths lower than *ca.* 380 nm, which indicated that the absorption was not due to the transition from the impurity level but was due to the band-gap transition[28]. The sample prepared at pH=11.00 have two steep shape, one was the bad-gap transition of $CdMoO_4$, the other may be the band-gap transition of $Cd(OH)_2$ [29].

The photocatalytic activities of the samples were evaluated by RhB degradation. The photodegradation efficiencies of RhB as a function of irradiation time for $CdMoO_4$ microcrystals under UV light illumination are depicted in Figure 6. At pH=5.00, the product derived at 180 °C for 24 h showed the best photocatalytic performance which can effectively degrade 89% RhB within 30 min. Moreover, the photocatalytic activities of $CdMoO_4$ products changed obviously with changing reaction temperature and time. However, the changes in the photocatalytic activities of $CdMoO_4$ products prepared under different pH are not significant. It is well-known that the photocatalytic activity of catalyst is related to its phase compositions, structures, and

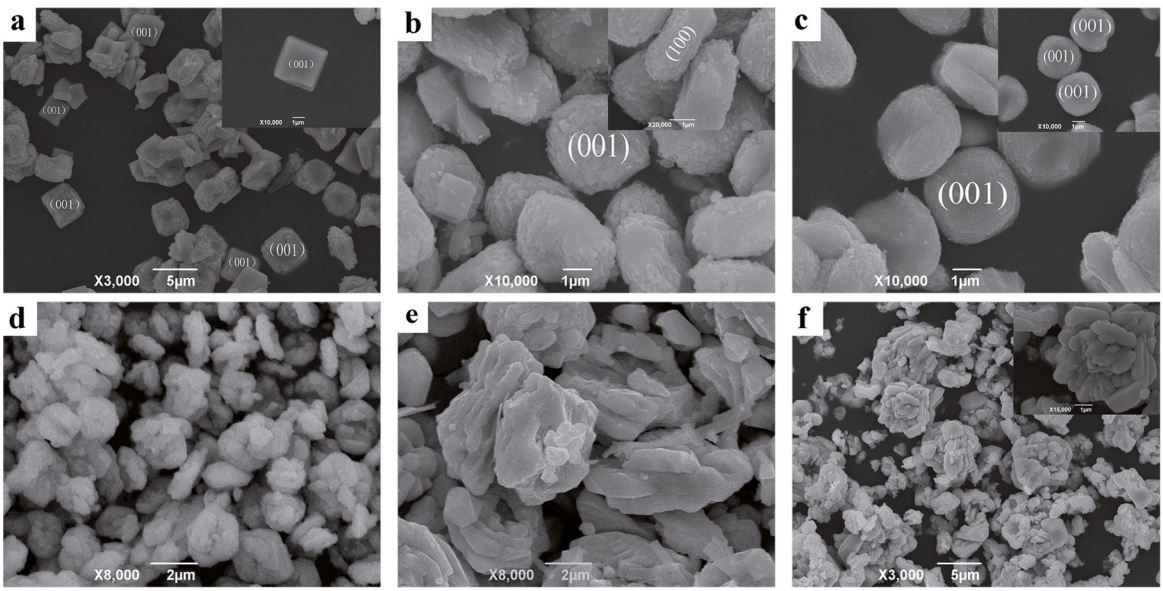

Figure 3: SEM images of $CdMoO_4$ products obtained at pH=5 and 180 °C for different hydrothermal times at 180 °C. (a) 1 h, (b) 4 h, (c) 8 h, (d) 16 h, (e) 24 h, and (f) 48 h.

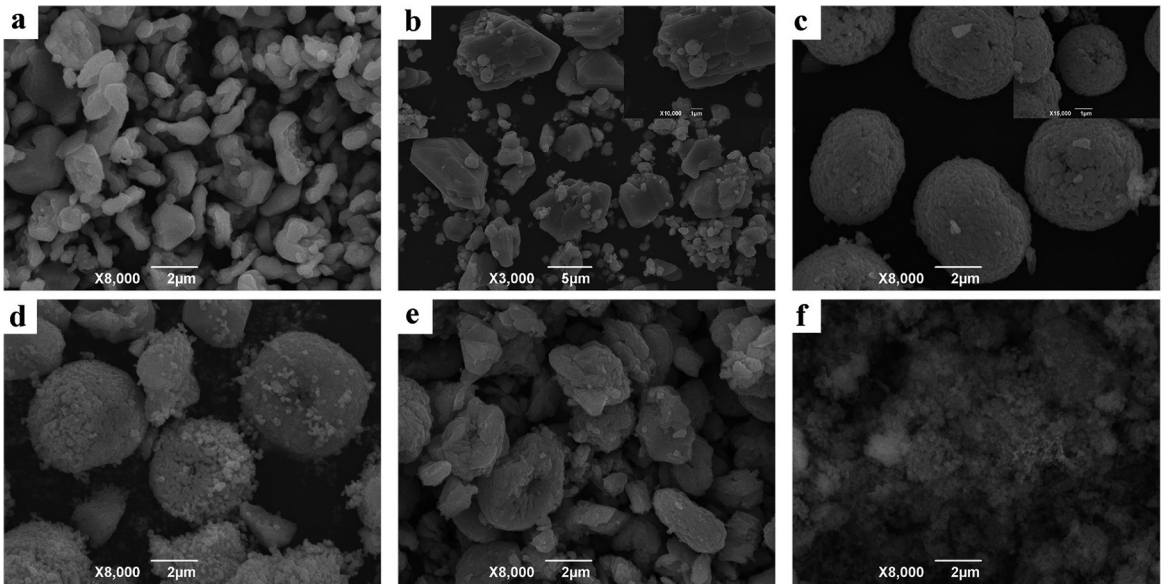

Figure 4: SEM images of $CdMoO_4$ products obtained for different pH for 24 h at 180 °C. (a) pH=1.73, (b) pH=3.00, (c) pH=5.00, (d) pH=7.00, (e) pH=9.00, and (f) pH=11.00.

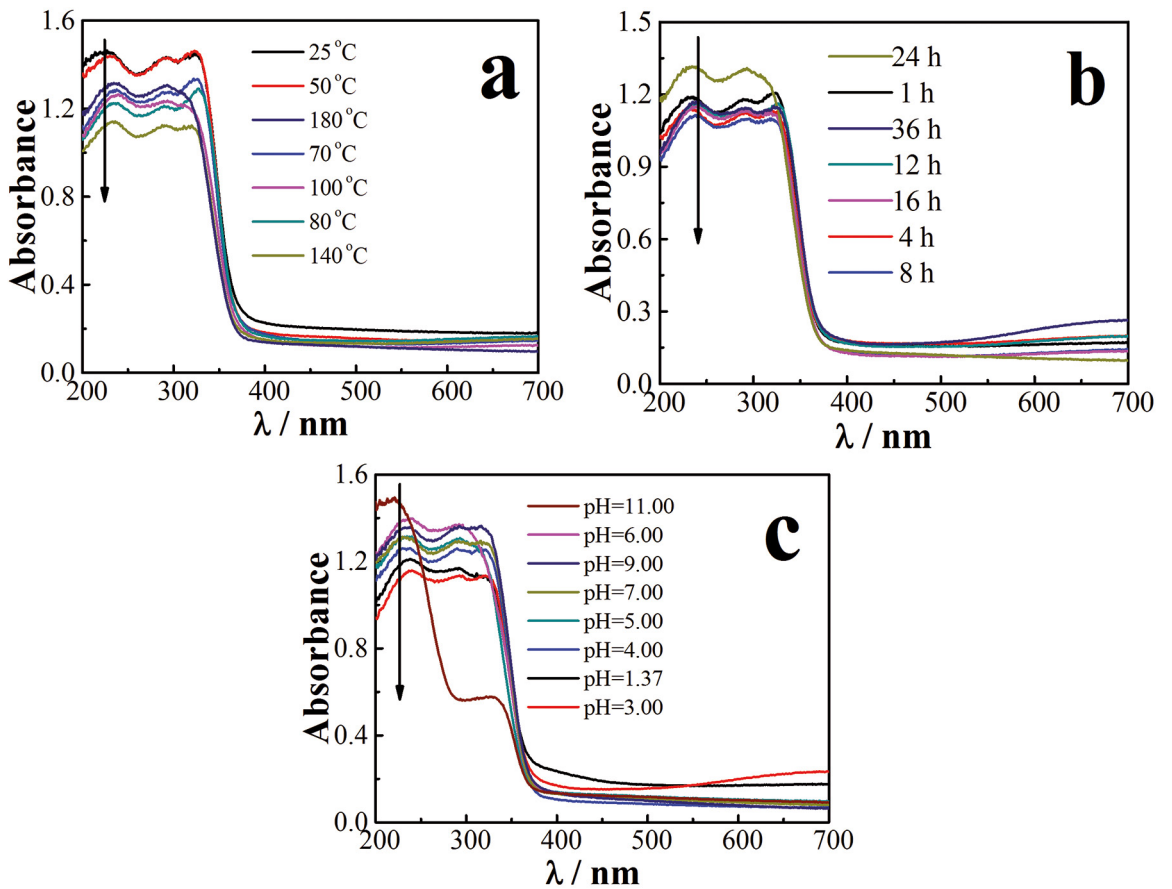

Figure 5: UV-vis diffuse reflectance absorption spectra of $CdMoO_4$ products. (a) temperature series at pH=5 for 24 h, (b) time series at pH=5 and 180 °C, and (c) pH series at 180 °C for 24 h.

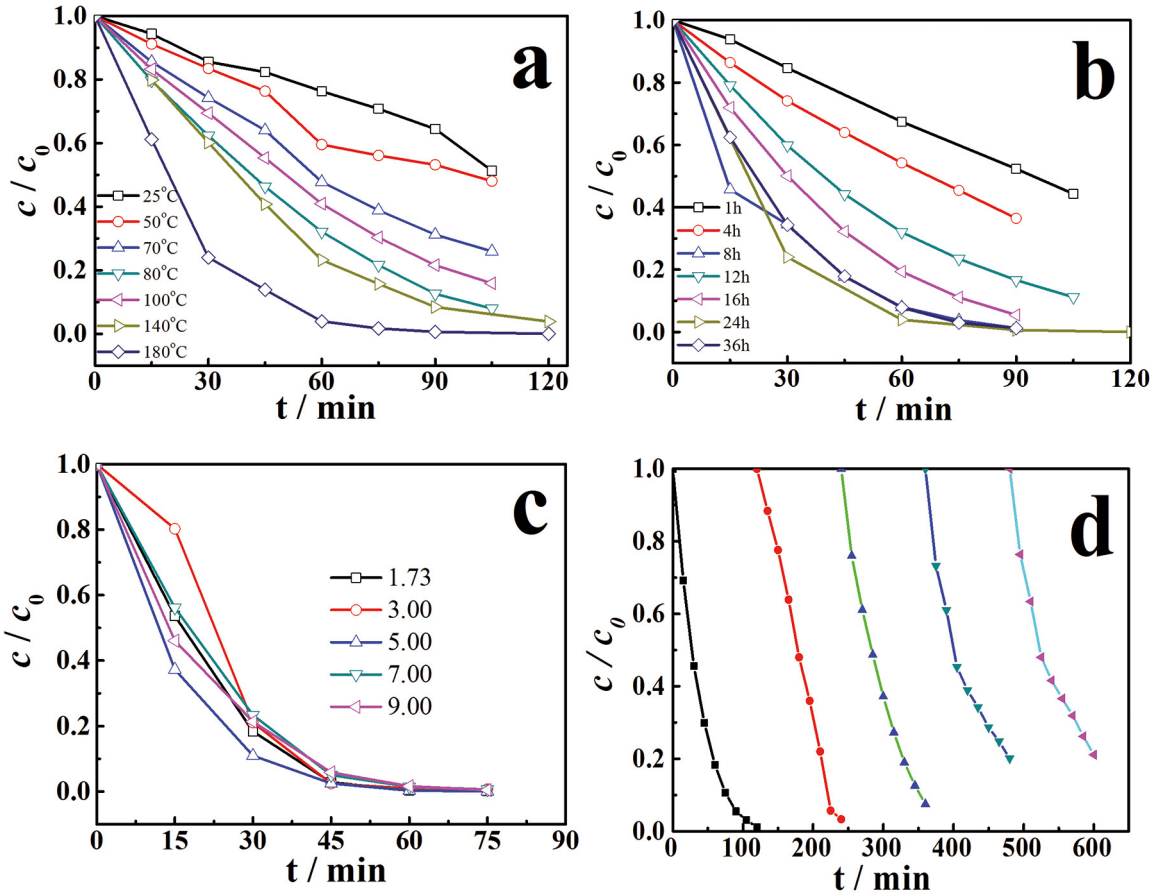

Figure 6: Photodegradation efficiencies of RhB as a function of irradiation time over $CdMoO_4$ products synthesized under various reaction conditions. (a) temperature series at pH=5 for 24 h, (b) time series at pH=5 and 180 °C, (c) pH series at 180 °C for 24 h, and (d) repeated experiment of RhB photodegradation over $CdMoO_4$ products.

morphologies, which are greatly influenced by the synthesis conditions[30-33]. It can be noticed that the photocatalytic activities of $CdMoO_4$ products are highly related to its crystallinity (Figure 1b-1d) except for the $CdMoO_4$ products prepared under different pH. Crystallinity has a certain effect on the photocatalytic activity. The higher the crystallinity, the fewer the bulk defects, and the higher the photocatalytic activity is. Therefore, the $CdMoO_4$ products with high crystallinity demonstrated excellent photocatalytic activity. On the other hand, the morphologies and exposed facets of photocatalyst are also important to its photocatalytic activity[34-36]. Based on the results of this study, the photocatalytic activity of $CdMoO_4$ is closely related to not only the crystallinity but also the facet.

The stability of a photocatalyst is also important for its applications. In this work, circulating runs in the photodegradation of RhB by $CdMoO_4$ micro-ellipsoids are examined under UV irradiation without washing the photocatalyst. The photoactivity of $CdMoO_4$ remains at 78% after 10 recycles of RhB photodegradation, as shown in Figure 6d, indicating that the prepared $CdMoO_4$ materials have moderate photostability.

3.4. Formation mechanism of $CdMoO_4$ micro-ellipsoids

The typical SEM images and XRD patterns of $CdMoO_4$ micro-ellipsoids prepared at 180 °C and pH 5.00 for 24 h are shown in Figure 7. The low-magnification SEM images in Figure 7a show that the product contains numerous micro-ellipsoids with a long axis of about 2-6 μm, indicating that micro-ellipsoids can be prepared on a large scale by the proposed easy method. One individual micro-ellipsoid (Figure 7b) is shown to have a well-defined ellipsoid 6 μm in size, and this ellipsoid is assembled by a nanotablet ~200 nm in size. The high-magnification SEM images further reveal that these micro-ellipsoids are actually composed of many plate-like microcrystals (Figure 7c). The XRD pattern of the micro-ellipsoids is displayed in Figure 7d. All diffraction peaks can be ascribed to scheelite-type tetragonal $CdMoO_4$ (JCPDS No. 07-0209), and no impurity peak can be observed, indicating the formation of pure scheelite-type tetragonal $CdMoO_4$.

To reveal the growth process of $CdMoO_4$ micro-ellipsoids, time-dependent experiments were conducted. The products were collected at different stages during the

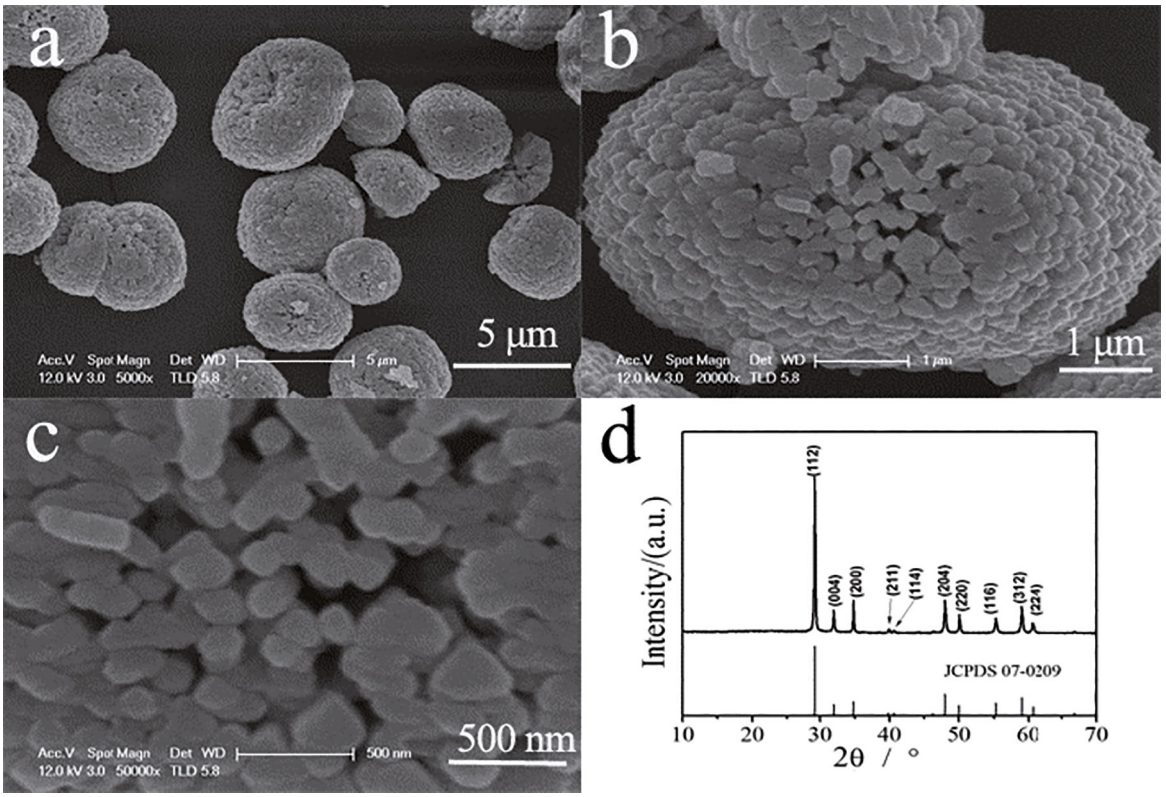

Figure 7: Typical SEM images with different magnifications (a-c) and XRD patterns (d) of $CdMoO_4$ products obtained at pH=5.00, 180 °C for 24 h.

reaction, and then their morphologies were investigated by SEM. The evolutionary stages are shown in Figure 8. After 1 h of hydrothermal reaction, products with microspheres and several nanoparticles are observed (Figure 8a). With prolonged reaction time to 4 h, only nanoparticles exist (Figure 8b); at 8 h, smaller nanoparticles are observed (Figure 8c). Further increased reaction time leads to the formation of bulk structures (Figure 8d), and then micro-ellipsoids are observed on the bulks (Figure 8e). Finally, when the reaction time is extended to 24 h, micro-ellipsoids were appearing (Figure 8f). However, when the reaction time is keeping for 48 h, microspheres and several nanoparticles are both observed (Figure 8g).

Based on the above observations, a schematic of the formation mechanism of $CdMoO_4$ ellipsoids is shown in Figure 9. In the first step, a cadmium molybdate crystal nucleus forms from molybdate ion and cadmium ions, and then an unstable globular structure forms. In the second step, this globular structure breaks into nanoparticles. In the third step, an irregular polyhedron structure forms at the expense of the small particles. In the fourth step, elliptic spherical structures grow on the irregular polyhedron, so the number of irregular polyhedrons decrease and the number of elliptic spherical structures increase. Finally micro-ellipsoids form. After a long time, stable spheres finally appear. The entire process that the $CdMoO_4$ crystals undergo is the Ostwald ripening process[37-39]. This spontaneous process occurs because larger particles are more energetically favored than smaller particles. The formation of many small particles is kinetically favored (i.e., they are more easily to nucleate). However, large particles are thermodynamically favored because small particles have a larger ratio of surface area to volume than large particles and are thus easier to produce. The competition between thermodynamics and kinetics drives the crystal-transformation process. Molecules on the surface are energetically less stable than the ones already well ordered and packed in the interior. Large particles, with their greater ratio of volume to surface area, thus have a lower energy state. Hence, many small particles attain a lower energy state if transformed into large particles. Finally the spheres and particles reach the equilibrium state.

4. Conclusions

$CdMoO_4$ micro-ellipsoids were synthesized at an initial hydrothermal pH of 5.00 and temperature of 180 °C for 24 h in the presence of Triton X-100. Comparative analysis of different series of $CdMoO_4$ materials reveals that hydrothermal temperature and time have a significant influence on the photocatalytic activity of $CdMoO_4$ than pH.

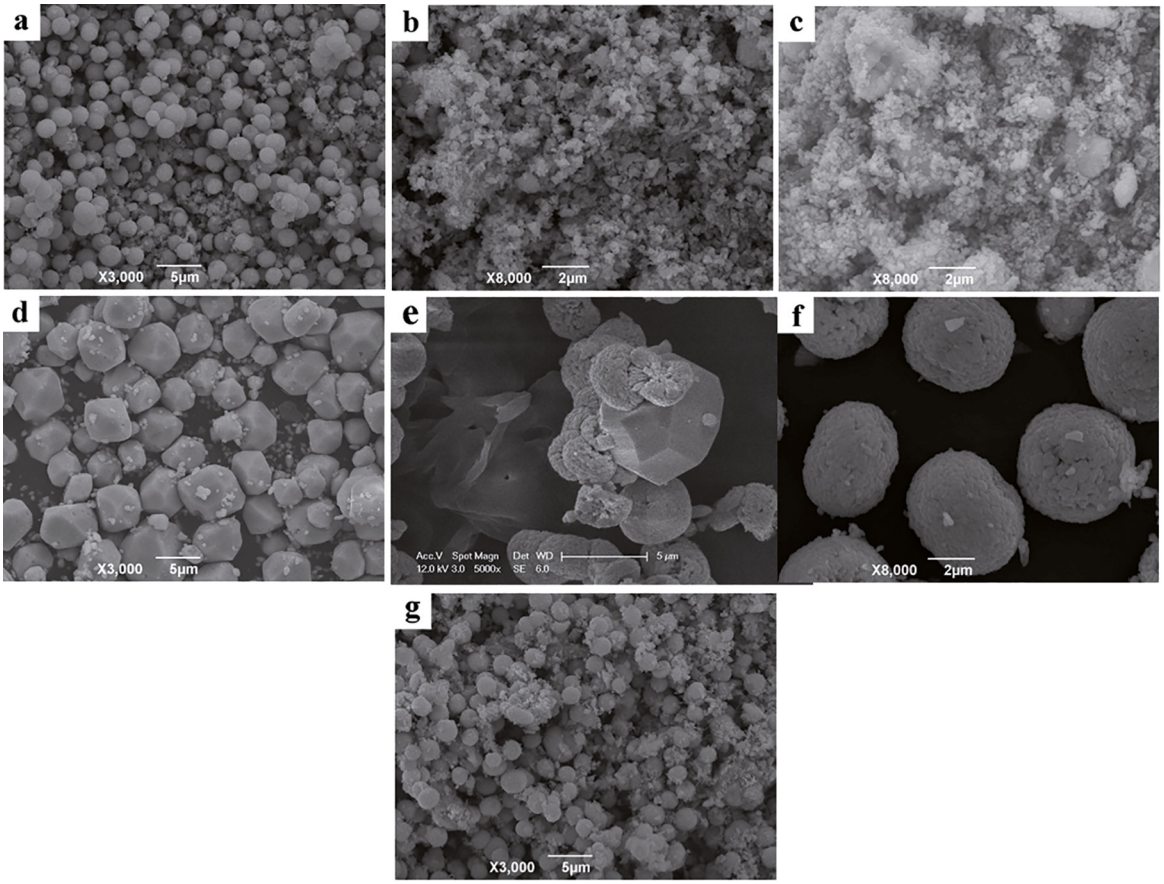

Figure 8: SEM images of $CdMoO_4$ products obtained at different hydrothermal times at pH=5.00, 180 °C. (a) 1 h, (b) 4 h, (c) 8 h, (d) 16 h, (e) 20 h, (f) 24 h, and (g) 48 h.

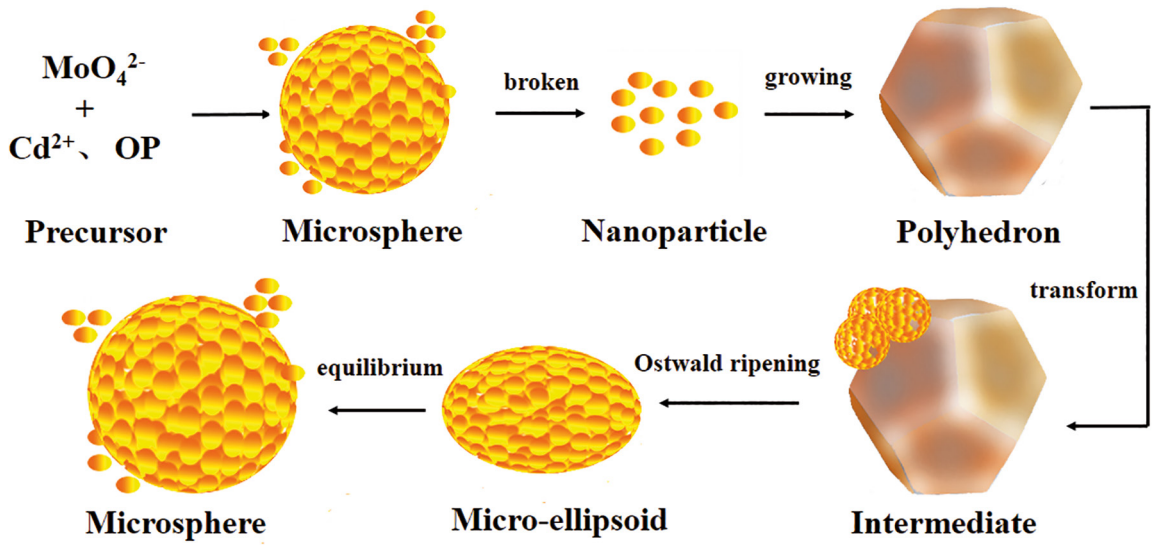

Figure 9: Schematic illustration of the growth process of $CdMoO_4$ micro-ellipsoids.

The crystal facet and crystallinity of $CdMoO_4$ play a key part in its photocatalytic activity. Moreover, the formation mechanism of $CdMoO_4$ micro-ellipsoids was investigated, which is related to an Ostwald ripening process. Notably, the $CdMoO_4$ micro-ellipsoids exhibit excellent photocatalytic activity for RhB degradation. This work may demonstrate a general method for synthesizing other photocatalytic materials with special morphology.

5. Acknowledgments

The research was financially supported by the National Natural Science Foundation of China (51572101) and the Fundamental Research Funds for Central Universities (2662015PY047) of China.

6. References

1. Dong M, Lin Q, Sun H, Chen D, Zhang T, Wu Q, et al. Synthesis of Cerium Molybdate Hierarchical Architectures and Their Novel Photocatalytic and Adsorption Performances. *Crystal Growth & Design*. 2011;11(11):5002-5009.

2. Zhang N, Liu S, Xu YJ. Recent progress on metal core@ semiconductor shell nanocomposites as a promising type of photocatalyst. *Nanoscale*. 2012;4(7):2227-2238.

3. Zhang L, Zhu Y. A review of controllable synthesis and enhancement of performances of bismuth tungstate visible-light-driven photocatalysts. *Catalysis Science & Technology*. 2012;2(4):694-706.

4. Li Y, Mi Y, Jiang J, Huang Z. Room-temperature Synthesis of $CdMoO_4$ Nanooctahedra in the Hemline Length of 30 nm. *Chemistry Letters*. 2010;39(7):760-761.

5. Zhang Q, Wang W, Goebl J, Yin Y. Self-templated synthesis of hollow nanostructures. *Nanotoday*. 2009;4(6):494-507.

6. Lin G, Zheng J, Xu R. Template-Free Synthesis of Uniform CdS Hollow Nanospheres and Their Photocatalytic Activities. *Journal of Physical Chemistry C*. 2008;112(19):7363-7370.

7. Sczancoski JC, Bomio MDR, Cavalcante LS, Joya MR, Pizani PS, Varela JA, et al. Morphology and Blue Photoluminescence Emission of $PbMoO_4$ Processed in Conventional Hydrothermal. *Journal of Physical Chemistry C*. **2009;**113(14):5812-5822.

8. Adhikari R, Gyawali G, Kim TH, Sekino T, Lee SW. Synthesis of Er^{3+} loaded barium molybdate nanoparticles: A new approach for harvesting solar energy. *Materials Letters*. 2013;91:294-297.

9. Carlsson PA, Jing D, Skoglundh M. Controlling Selectivity in Direct Conversion of Methane into Formaldehyde/Methanol over Iron Molybdate via Periodic Operation Conditions. *Energy & Fuels*. 2012;26(3):1984-1987.

10. Zhang M, Shao C, Zhang P, Su C, Zhang X, Liang P, et al. Bi_2MoO_6 microtubes: Controlled fabrication by using electrospun polyacrylonitrile microfibers as template and their enhanced visible light photocatalytic activity. *Journal of Hazardous Materials*. 2012;225-226:155-163.

11. Shen M, Zhang X, Dai K, Chen H, Peng T. Hierarchical $PbMoO_4$ microspheres: hydrothermal synthesis, formation mechanism and photocatalytic properties. *CrystEngComm*. 2013;15:(6):1146-1152.

12. Mikhailik VB, Kraus H, Wahl D, Mykhaylyk MS. Studies of electronic excitations in $MgMoO_4$, $CaMoO_4$ and $CdMoO_4$ crystals using VUV synchrotron radiation. *Physica Status Solidi (B)*. 2005;242(2):R17-R19.

13. Jayaraman A, Wang SY, Sharma SK. High-pressure Raman investigation on $CdMoO_4$ and pressure-induced phase transformations. *Physical Review B*. 1995;52(14):9886-9889.

14. Adhikari R, Malla S, Gyawali G, Sekino T, Lee SW. Synthesis, characterization and evaluation of the photocatalytic performance of Ag-$CdMoO_4$ solar light driven plasmonic photocatalyst. *Materials Research Bulletin*. 2013;48(9):3367-3373.

15. Madhusudan P, Zhang J, Cheng B, Yu J. Fabrication of $CdMoO_4$@ CdS core–shell hollow superstructures as high performance visible-light driven photocatalysts. *Physical Chemistry Chemical Physics*. 2015;17(23):15339-15347.

16. Ren Y, Ma J, Wang Y, Zhu X, Lin B, Liu J, et al. Shape-Tailored Hydrothermal Synthesis of $CdMoO_4$ Crystallites on Varying pH Conditions. *Journal of the American Ceramic Society*. 2007;90(4):1251-1254.

17. Wang WS, Zhen L, Xu CY, Shao WZ, Chen ZL. Formation of $CdMoO_4$ porous hollow nanospheres *via* a self-assembly accompanied with Ostwald ripening process and their photocatalytic performance. *CrystEngComm*. 2013;15(39):8014-8021.

18. Khademolhoseini S, Zakeri M, Rahnamaeiyan S, Nasiri M, Talebi R. A simple sonochemical approach for synthesis of cadmium molybdate nanoparticles and investigation of its photocatalyst application. *Journal of Materials Science: Materials in Electronics*. 2015;26(10):7303-7308.

19. Wang W, Cui J, Wang P, Zhen L, Shao W, Chen Z. Self-supported construction of 3D $CdMoO_4$ hierarchical structures from nanoplates with enhanced photocatalytic properties. *RSC Advances*. 2014;4(73):38527-38534.

20. Li D, Zhu Y. Synthesis of $CdMoO_4$ microspheres by self-assembly and photocatalytic performances. *CrystEngComm*. 2012;14(3):1128-1134.

21. Gong Q, Li G, Qian X, Cao H, Du W, Ma X. Synthesis of single crystal $CdMoO_4$ octahedral microparticles via microemulsion-mediated route. *Journal of Colloid and Interface Science*. 2006;304(2):408-412.

22. Wang WS, Zhen L, Xu CY, Shao WZ. Room Temperature Synthesis, Growth Mechanism, Photocatalytic and Photoluminescence Properties of Cadmium Molybdate Core−Shell Microspheres. *Crystal Growth & Design*. 2009;9(3):1558-1568.

23. Liu H, Tan L. Synthesis, structure, and electrochemical properties of $CdMoO_4$ nanorods. *Ionics*. 2010;16(1):57-60.

24. Yu J, Wang B. Effect of calcination temperature on morphology and photoelectrochemical properties of anodized titanium dioxide nanotube arrays. *Applied Catalysis B: Environmental*. 2010;94(3-4):295-302.

25. Shamaila S, Sajjad AKL, Chen F, Zhang J. Mesoporous titania with high crystallinity during synthesis by dual template system as an efficient photocatalyst. *Catalysis Today.* 2011;175(1):568-575.

26. McLaren A, Valdes-Solis T, Li G, Tsang SC. Shape and size effects of ZnO nanocrystals on photocatalytic activity. *Journal of the American Chemical Society*. 2009;131(35):12540-12541.

27. Umar A, Ribeiro C, Al-Hajry A, Masuda Y, Hahn YB. Growth of highly c-axis-oriented ZnO nanorods on ZnO/glass substrate: growth mechanism, structural, and optical properties. *Journal of Physical Chemistry C*. 2009;113(33):14715-14720.

28. Kudo A, Tsuji I, Kato H. $AgInZn_7S_9$ solid solution photocatalyst for H_2 evolution from aqueous solutions under visible light irradiation. *Chemical Communications*. 2002;17:1958-1959.

29. Gujar TP, Shinde VR, Kim WY, Jung KD, Lokhande CD, Joo OS. Formation of CdO films from chemically deposited $Cd(OH)_2$ films as a precursor. *Applied Surface Science*. 2008;254(13):3813-3818.

30. Dai K, Yao Y, Liu H, Mohamed I, Chen H, Huang Q. Enhancing the photocatalytic activity of lead molybdate by modifying with fullerene. *Journal of Molecular Catalysis A: Chemical*. 2013;374-375:111-117.

31. Zhu H, Wang J, Wu D. Fast Synthesis, Formation Mechanism, and Control of Shell Thickness of CuS Hollow Spheres. *Inorganic Chemistry*. 2009;48(15):7099-7104.

32. Shen M, Zhang Q, Chen H, Peng T. Hydrothermal fabrication of $PbMoO_4$ microcrystals with exposed (001) facets and its enhanced photocatalytic properties. *CrystEngComm*. 2011;13(7):2785-2791.

33. D'Arienzo M, Carbajo J, Bahamonde A, Crippa M, Polizzi S, Scotti R, et al. Photogenerated Defects in Shape-Controlled TiO_2 Anatase Nanocrystals: A Probe To Evaluate the Role of Crystal Facets in Photocatalytic Processes. *Journal of the American Chemical Society*. 2011;133(44):17652-17661.

34. Pan J, Liu G, Lu GQ, Cheng HM. On the True Photoreactivity Order of {001}, {010}, and {101} Facets of Anatase TiO_2 Crystals. *Angewandte Chemie International Edition*. 2011;50(9):2133-2137.

35. Han X, Kuang Q, Jin M, Xie Z, Zheng L. Synthesis of titania nanosheets with a high percentage of exposed (001) facets and related photocatalytic properties. *Journal of the American Chemical Society*. 2009;131(9):3152-3153.

36. Yang HG, Sun CH, Qiao SZ, Zou J, Liu G, Smith SC, et al. Anatase TiO_2 single crystals with a large percentage of reactive facets. *Nature*. 2008;453:638-641.

37. Bastús NG, Comenge J, Puntes V. Kinetically controlled seeded growth synthesis of citrate-stabilized gold nanoparticles of up to 200 nm: size focusing versus Ostwald ripening. *Langmuir*. 2011;27(17):11098-11105.

38. Mahesh S, Gopal A, Thirumalai R, Ajayaghosh A. Light-induced Ostwald ripening of organic nanodots to rods. *Journal of the American Chemical Society*. 2012;134(17):7227-7230.

39. Johnson NJJ, Korinek A, Dong C, van Veggel FCJM. Self-Focusing by Ostwald Ripening: A Strategy for Layer-by-Layer Epitaxial Growth on Upconverting Nanocrystals. *Journal of the American Chemical Society*. 2012;134(27):11068-11071.